Fast Timing Via Cerenkov Radiation: A simulation study

Earle Wilson
Morehouse College

***Abstract*: High precision timing will be a critical requirement for the next generation of high energy particle physics experiments. In particular, high precision timing will be essential for forward proton detectors in the FP420 experiment at the LHC. Collaborators behind the FP420 project have proposed the idea of positioning proton detectors 420m away from the CMS/ATLAS points of interaction. These detectors will serve as secondary detectors to tag protons scattered at very small angles with fractional longitudinal momentum loss of less than 2%. To associate scattered protons with their correct point of interaction, timing resolution on the order of a few picoseconds will be needed. This paper presents a simulation study that explores the possibility of having detectors capable of picosecond timing. The simulation of the detector was done using Geant 4 and the analysis was done using ROOT both written in C++. Two very different detector types were studied: one detector used a quartz bar as a radiator for cerenkov photons, the other detector used aerogel as a radiator. We studied the effects contributing most to the timing resolution like the photon statistics, light dispersion in the case of the quartz bar radiator and rayleigh scattering in the case of the aerogel radiator, quantum efficiency and spectral response of the photo detectors etc. The results we obtained were compared with test beam results as well as with the results of groups working on similar projects. Our studies demonstrated that sufficient time resolution could be achieved satisfying the requirements of the experiment and allowed us to optimize the detector design.**

I. INTRODUCTION

Collaborators behind the FP420 project have proposed the idea of positioning two proton detectors 420m away from the CMS/ATLAS point of interactions at the Large Hardon Collider (LHC) in Cern [1]. These detectors will serve as secondary detectors to tag protons scattered at very small angles with fractional longitudinal momentum loss of less than 2% [1]. Measurement of the angular displacement and the displacement from the beam line will allow for the measurement of these scattered protons [1]. Detection of these forward protons is expected to open up new studies of Quantum Chromodynamics, Higgs Boson, electroweak physics and additional physics beyond the standard model [1]. The challenge of detecting these forward protons lies in the high luminosity and fast bunch crossing rate of the proton bunches. Hence, to associate scattered protons with their correct point of interaction, timing resolution on the order of 10 picoseconds is needed [1].

My main project this summer was to conduct simulation studies, using the Geant4 toolkit and the ROOT analysis program, to explore the possibilities of using quartz and aerogel to obtain picosecond timing resolution. Two different Geant4 simulations were set-up: one for a single quartz bar and another for multiple aerogel blocks. For the case of the quartz bar, photon statistics such as wavelength and energy spectra, the prevalence of secondary photons, the effects of varying the angle of the incident proton beam and the effects of dispersion were studied. The effect of varying the size of the bar and the position of the beam was also studied. For the case of the aerogel radiator, similar aspects of photon statistics were investigated and the effect of Rayleigh scattering was studied for various numbers of aerogel blocks.

II. THEORY

Cerenkov radiation presents itself as a very suitable means for high precision timing as it is generated instantaneously whenever a charged particle traverses an insulating medium at a speed faster than the speed of light in that medium. When a charged particle, a proton for example, passes through a dielectric material at a speed greater than the speed of light in that medium, it disrupts the medium's electromagnetic field in such a way that a photon is promptly emitted. The emitted a photon emerges at an angle that is dependent on the refractive index in the following relationship:

$$\cos\theta = 1/\beta n \quad (1)$$

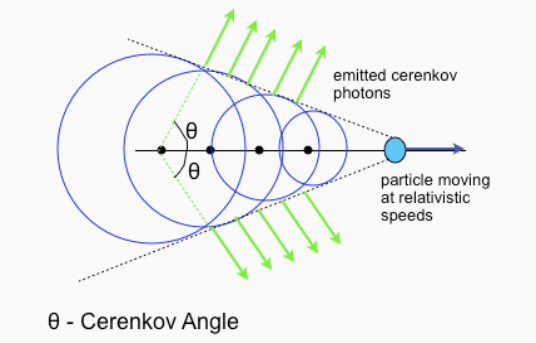

Fig.1: A diagram showing the creation of cerenkov light.

where theta is known as the cerenkov angle (see figure 1), n is the refractive index of the material, and β being the velocity of light in the medium (v) over speed of light in vacuum (c). The emitted cerenkov radiation is continuous and in a dispersive medium, the cerenkov angle is dependent on the wavelength. The number of photons emitted at a particular wavelength is given by the following equation:

$$n_{photons} = 2\pi\alpha L \sin^2\theta \int_{\lambda_2}^{\lambda_1} \frac{1}{\lambda^2} d\lambda \quad (2)$$

Where λ_1 and λ_2 represent the upper and lower limits of a given wavelength range, L is the length of the material traversed by the incident particle and α is a constant.

Given a charged particle with sufficient momentum, it is possible for that particle to collide with another particle inside the medium, causing the latter to acquire enough energy to move at a speed fast enough to emit its own cerenkov photons. In the case of interest, a proton moving at relativistic speeds can collide with an electron, known as a delta electron, which then emits its own cerenkov photons, known as secondary photons. These secondary photons are not accounted for by equation (2), which only predicts primary photons (photons that come directly from the incident particle).

For our simulations, we plan to direct a beam of protons moving at relativistic speeds through a given radiator, detect the emitted cerenkov light and obtain a timing resolution. The light of particular interest is the cerenkov light that comes from the incident proton. One foreseeable limitation to obtaining a precise timing resolution could be the presence of light emitting delta electrons as it may be possible for a significant amount of secondary photons to arrive at the detectors before the primary photons and skew the timing resolution results.

III. MATERIALS AND METHODS

Simulations and analyses were conducted using Geant4, a C++ based Monte Carlo program, and ROOT, a C++ based analysis program [2,3]. For both simulations the following physics processes were included in Geant4: electromagnetic physics, Cerenkov radiation, absorption, and multiple scattering. In addition, dispersion and rayleigh scattering were added to the quartz bar and aerogel simulations respectively. The physical processes originating from the radiating material were simulated using Geant4, which output a ROOT file for analysis. The physical processes of the detector were simulated using ROOT, which also output a ROOT file for analysis.

i. *Quartz Bar Simulation*

The material properties of quartz are described in figures 2 and 3. Figure 2 shows the absorption lengths of quartz bar for the 150 - 700 nm wavelength range. In particular, figure 2 shows that quartz is most absorptive in the blue/ultraviolet range of wavelength spectrum. Figure 3, shows the dispersion properties of quartz. The plot shows that photons at the red end of the wavelength spectrum travel through quartz faster than those at the blue end of the wavelength spectrum. One should also note the significant change in refractive indices within the 150 - 250 nm range.

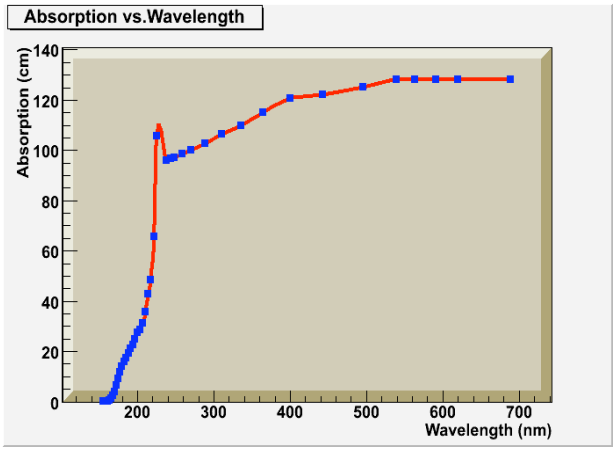

Figure 2: Absorption against wavelength for aerogel.

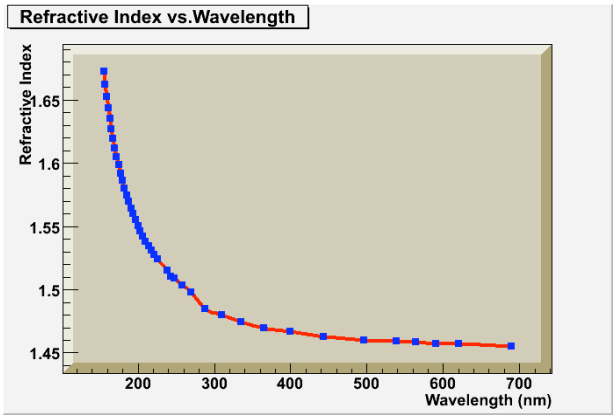

Figure 3: Refractive index against wavelength for aerogel

For the initial setup (see figure 4), a 6 mm x 6 mm by 9 cm solid bar made of Quartz (SiO_2) was used. An incident beam of 7 TeV protons was directed at the center of the quartz at an angle perpendicular to the bar. As the proton traverses the quartz medium it will emit cerenkov radiation at an angle for a given refractive index. Some of the emitted photons will travel along the length of the quartz bar by way of total internal reflection until they meet one of two photo-sensitive detectors located at either ends of the bar. For the initial set up, Hamamatsu MCP-PMT R3809U-65 detectors were used. The Hamamatsu was later substituted by the Photek 240 PMT detector.

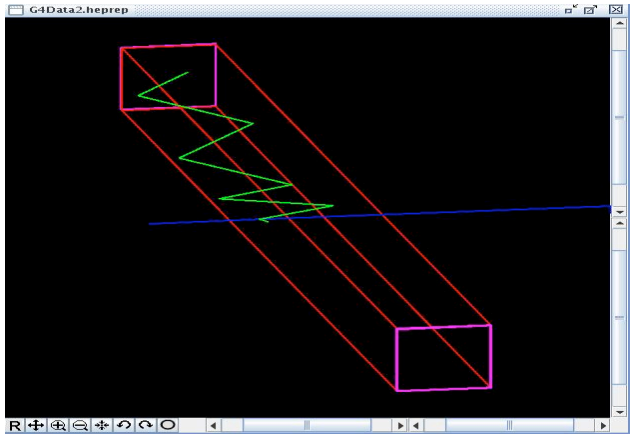

Figure 4: A simple diagram showing the initial set up of the quartz bar simulation. The blue line represents the incident proton beam. The green line is an example of a cerenkov photon traveling along the length of the quartz bar.

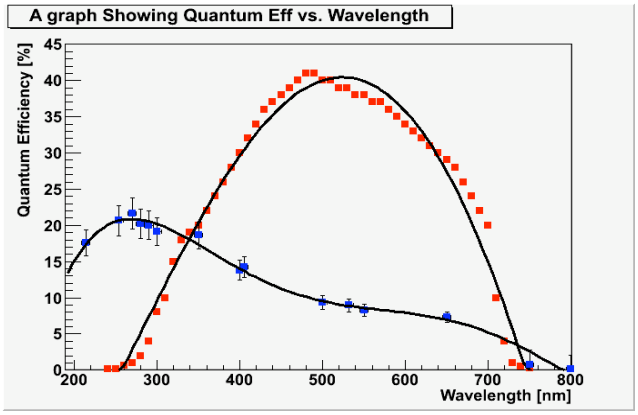

Figure 5: This is a graph showing the quantum efficiencies for the Hamamatsu MCP R3809U-65 (red) and the Photek 240 (blue).

The quantum efficiencies of the Hamamatsu and Photek detectors as a function of wavelength are shown in figure 5. For the sake of computing time, a gain of only 100 was implemented, though the gain of the actual detectors can be of the order of 10^6. The simulation assumed a time transit spread of the photoelectrons to be 30 picoseconds. Several simulations were conducted for this set-up and the results were analyzed and noted. Analyses were taken at different stages of the simulation. First, an analysis of the cerenkov photons and delta electrons were taken at the moment of creation. The properties and statistics of the emitted cerenkov radiation with detailed account of the presence of delta electrons were investigated. Second, an analysis of the emitted photons was taken just before and after they are collected at the detectors. At this point, the properties and statistics of the observed photons were taken investigated as well as their arrival time, their spatial distribution and timing resolution.

ii. *Obtaining the timing resolution: The Differentiated Center of Gravity (DCOG) method*

The timing resolution was obtained using a method known as the differentiated center of gravity (DCOG). The DCOG method begins by differentiating the leading edge of a histogram of the arrival time of photoelectrons (figures 6 and 7). The time corresponding to the center of gravity of the differentiated leading edge is obtained for a number of events (figure 8) and the time spread is fit with a Gaussian function. The mean of the Gaussian is taken as the average arrival time and the standard deviation of the fit is taken as the timing resolution (figure 9). In the coding of this process, the leading edge is selected by employing two parameters. The first parameter defines a threshold for the difference in bin contents (i.e. number of photoelectrons) between successive bin and the second parameter is a threshold for the sum of the bin difference. These thresholds are established to avoid false triggers that can be caused by small peaks preceding the main peak of interest.

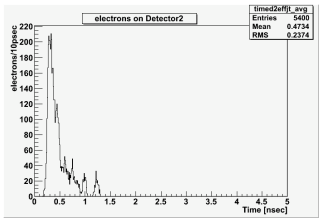

Figure 6: A histogram of the arrival time of electrons at the detector. The timing resolution is obtained from the leading edge.

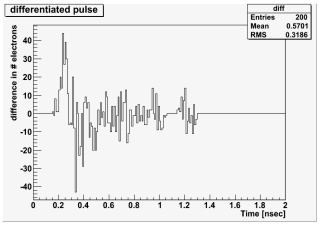

Figure 7: The differentiated plot of figure 6. The leading edge is represented by the first major peak.

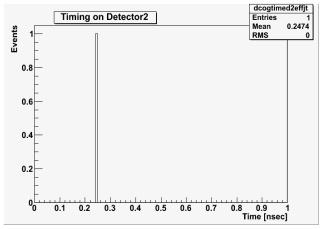

Figure 8: The time corresponding to the center of gravity of the first peak. This time is taken as the arrival time.

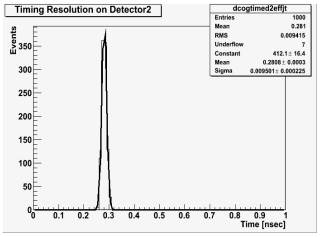

Figure 9: The arrival time is obtained for 1000 events and the standard deviation is taken as the timing resolution.

Once the timing resolution was obtained for the initial set-up, the angle of the incident beam was varied as shown in figure 10. Of particular interest was obtaining an alignment such that most of the primary photons travel to one of the detectors in a straight line, which would prevent the early arriving secondary photons from skewing the timing resolution. This was achieved by setting the angle of incidence of the proton beam at approximately 48 degrees. The angle of the incident beam was varied from 0 degrees, where the beam is perpendicular to the bar, to 70 degrees (from the normal). The number of photoelectrons at each detector and corresponding timing resolution was obtained for each angle.

After varying the angle of the incident beam, the dispersion effects of the quartz bar were added using the relationship showed in figure 3. The Hamamatsu was replaced by the Photek detector and its light collection efficiency (LCE) was taken into

account. The Photek was assumed to have a LCE of 60%. The simulation was repeated with the angle of the incident proton beam set at the cerenkov angle. The photon spectrum at the detector, number of photoelectrons per event, the average arrival time and the timing resolution was obtained. The next step in the simulations was to vary the dimensions of the quartz bar. The length of the quartz bar was varied from 10 cm to 20 cm and the thickness of the quartz bar was varied from 5 mm to 10 mm. The number of photoelectrons per event and timing resolution was obtained for each case. The final step in the quartz bar simulation was to vary the incident beam position at the cerenkov angle. The position of the beam was varied +/- 25 mm from the center in both the x and y plane and the number of photoelectrons per event and timing resolution was obtained.

iii. *Results of Quartz Bar Simulations*

This section describes the results of the quartz bar simulations done with initial set up of a 6 x 6 mm x 9 cm quartz bar, traversed by a beam of incident protons at an angle perpendicular to the quartz bar. For the initial simulations, a constant refractive index of 1.5 was assumed for all wavelengths. Figure 10 is a histogram showing the wavelength distribution of created cerenkov photons for 1000 events (1000 protons). The red curve shows the simulated wavelength distribution and blue curve shows the calculated wavelength distribution. While the two curves are very closely related, the Geant4 simulation predicts slightly more photons than the calculated number of photons. Fig. 11 shows a similar histograms but with the distinction between primary photons (cerenkov photons originating from the incident proton beam) and secondary photons (cerenkov photons originating from delta electrons). Here we see a better correlation between the Geant4 simulation and the theoretical calculation.

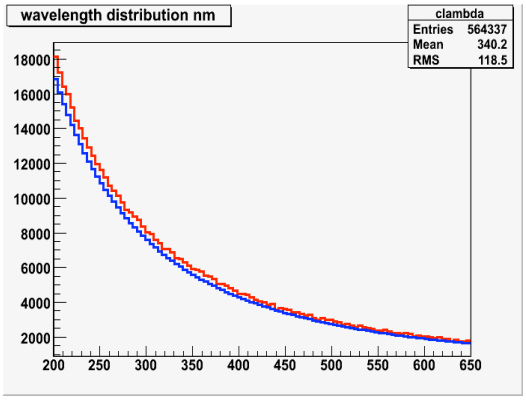

Figure 10: A wavelength spectrum of the created photons. The red line is the simulated photon spectrum and the blue line is the calculated wavelength spectrum using equation 2.

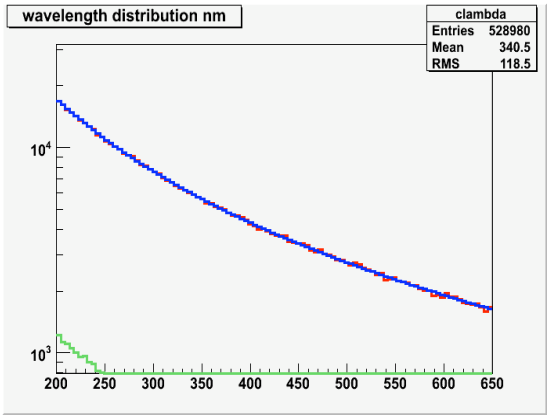

Fig 11: Wavelength spectrum of the created photons with the red line being the simulated photons, the blue line being the primary photons and the green line being the secondary photons.

Figure 12 is a histogram describing the prevalence of primary and secondary photons for each event. The distribution of primary photons per event is illustrated by the red curve, which is over-plotted with a Gaussian fit while the secondary photons are represented by the blue lines. Here we observe that approximately 85% of the simulated events have no secondary photons. Of the remaining events, seemingly arbitrary distribution of secondary photons are created per event. One should note that cases where the number of secondary photons is greater than that of the primary photons.

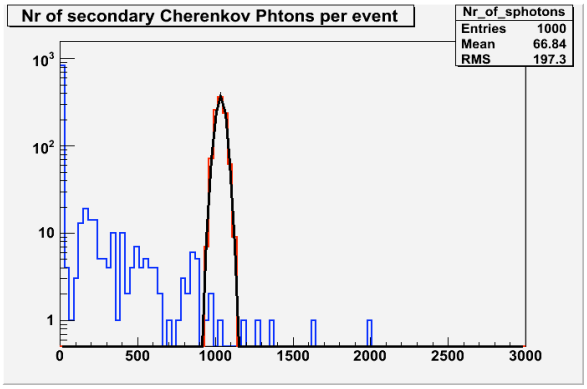

Figure 12: A histogram showing the number of primary (red line) and secondary photons (blue line) per event.

The next step was to observe the effects of changing the angle of the incident beam. This can be achieved by directing the proton beam at an angle equal to the cerenkov angle. Figure 13 shows the average number of photoelectrons as a function of angle of incidence for both the Hamamatsu and Photek detectors. Here we observe that the number of photoelectrons detected increases with the angle of incidence. Also, one observes that the Photek detector produces more photoelectrons at each angle than the Hamamatsu even though the Hamamatsu has a higher average quantum efficiency.

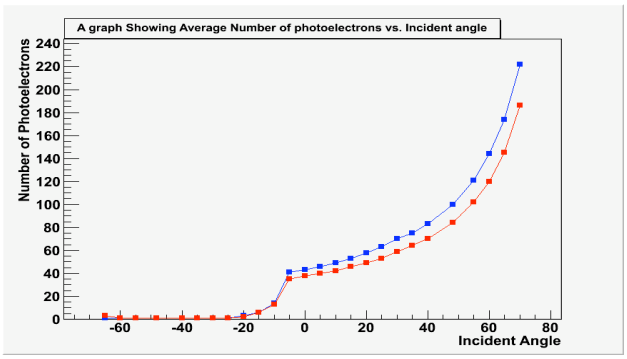

Figure 13: The average number of photoelectron against incident angle for the Hamamatsu (red line) and the Photek 240 (blue line).

Figure 14 and figure 15 illustrate the arrival time and timing resolution against incident angle for both the Hamamatsu and the Photek detector. Here the arrival time decreases as angle of incidence approaches the cerenkov angle but increases past 48 degrees for both detectors. The timing resolution also goes down as the angle increases but continues to decrease pass the cerenkov angle with the Photek 240 consistently producing a better timing resolution at each angle. The best timing resolution was approximately 2.8 picoseconds at around 65 degrees for the Photek 240.

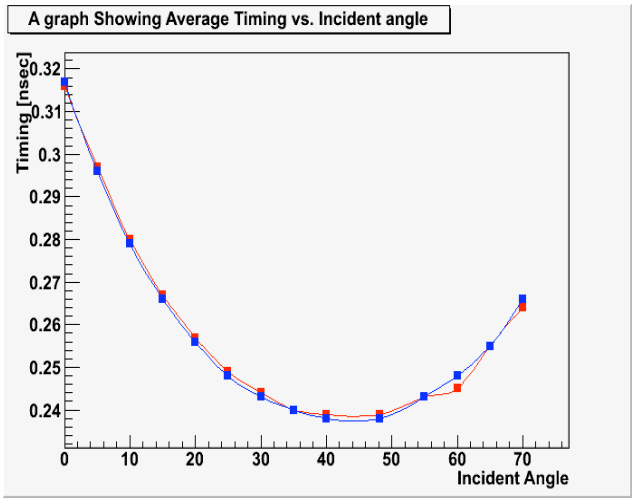

Figure 14: The average arrival time of photoelectrons as detected by the Hamamatsu (red) and the Photek 240 (blue). The fastest arrival time of about 0.24 nanoseconds is observed at around 48 degrees.

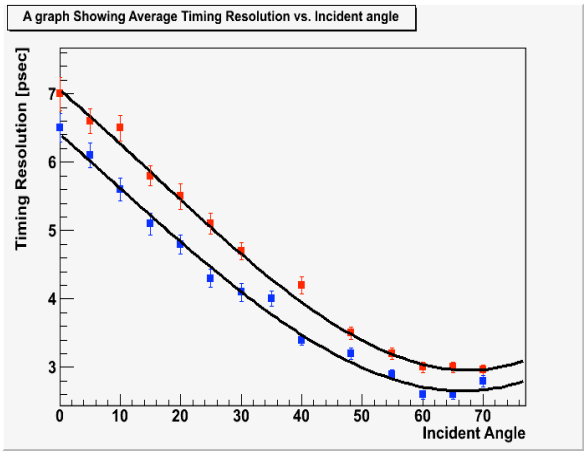

Figure 15: A graph showing the timing resolution against incident angle for the Hamamatsu (red) and Photek 240 (blue).

Figure 16 through figure 17 show the results after adding dispersion and light collection efficiency to the simulations. Figure 16 shows the timing resolution without dispersion and perfect light collection efficiency. Fig. 17 shows the timing resolution with dispersion and 60% light collection efficiency.

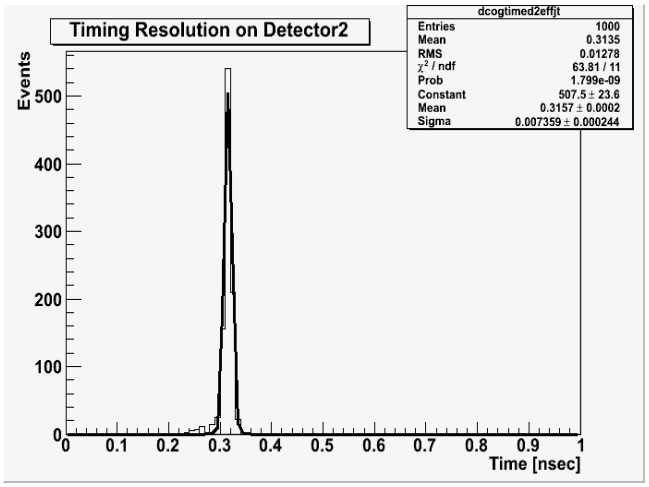

Figure 16: This plot shows the spread of arrival times for the case of no dispersion and perfect light collection efficiency. The standard deviation is approximately 7 picoseconds.

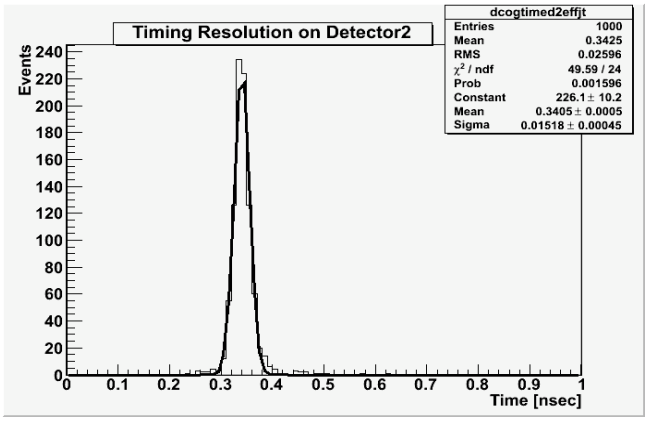

Figure 17: This plot shows the spread of arrival times for the case of dispersion and 60% light collection efficiency. The standard deviation is approximately 15 picoseconds.

Figure 18 through figure 21 show the results of varying the dimension of the quartz bar. Figure 18 shows the number of photoelectrons versus the thickness of the quartz bar. Here one can see a gradual increase in the number of photoelectrons as the thickness of the quartz bar is increased. Fig. 19 shows the simulated timing resolution against bar thickness and, as expected, the timing resolution improves with increased bar thickness. Figures 20 and 21 show the effects of varying the bar length on the number of photoelectrons detected and the subsequent timing resolution. Here one can see that number of photoelectrons decreases and as a consequence the timing resolution gets worse.

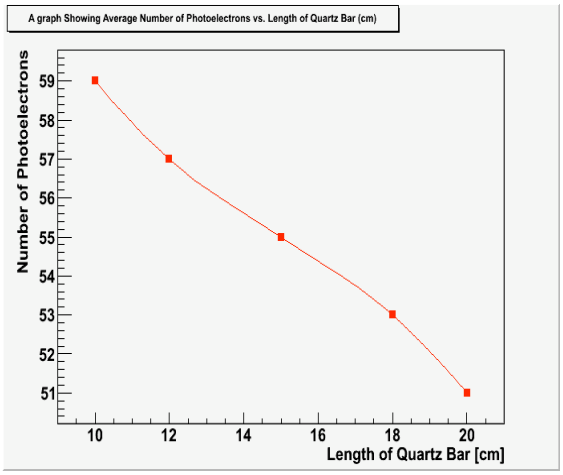

Figure 18: Number of photoelectrons versus the length of the quartz bar.

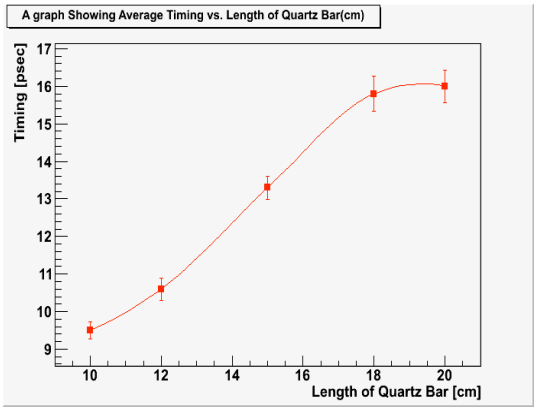

Figure 19: Timing resolution versus the length of the quartz bar.

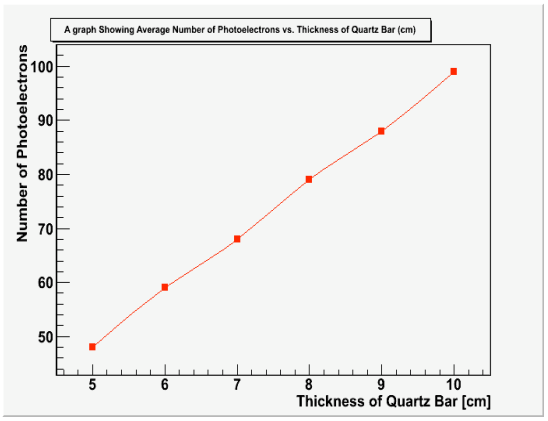

Figure 20: Average number of photoelectrons versus thickness of quartz bar.

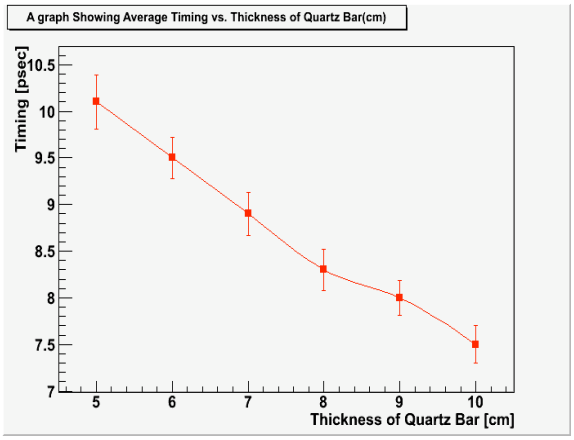

Figure 21: Timing resolution versus thickness of quartz bar.

Figure 22 through figure 25 shows the effect of varying the position of the incident beam. Figure 22 and figure 23 show the effect of varying the position of the beam along the x plane (horizontally) on the number of photoelectrons and the timing resolution. Here one sees that number of photoelectrons remain almost constant at approximately 98 and, as a result, no significant changes in the timing resolution was observed. Figure 24 and figure 25 show the effect of varying the position of the beam along the y plane (vertically) on the number of photoelectrons and the timing resolution. Once again, the number of photoelectrons remain roughly constant for the given position variation and, as a result, there was very little change in the timing resolution.

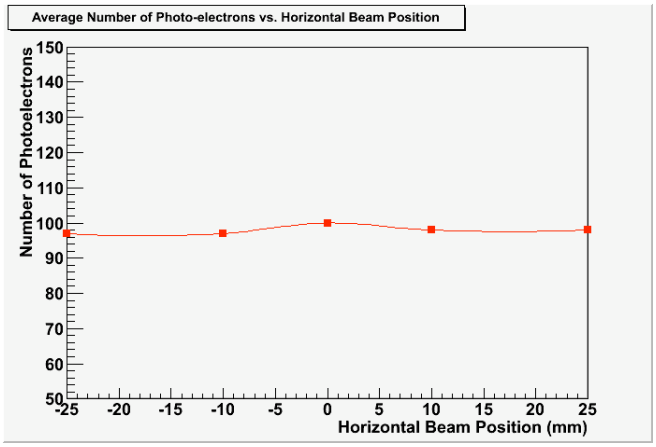

Figure 22: Number of photoelectrons versus horizontal beam position.

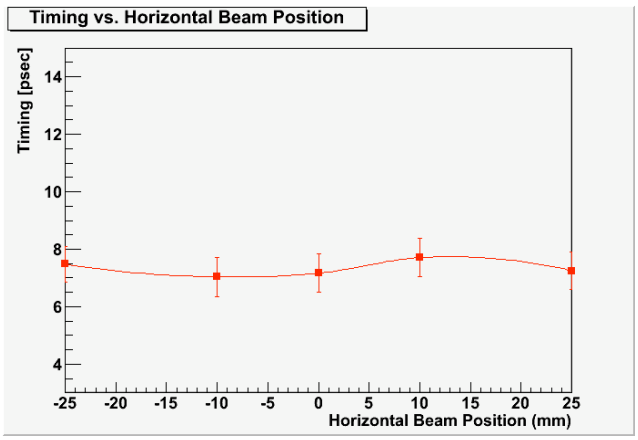

Figure 23: Timing resolution versus horizontal beam position.

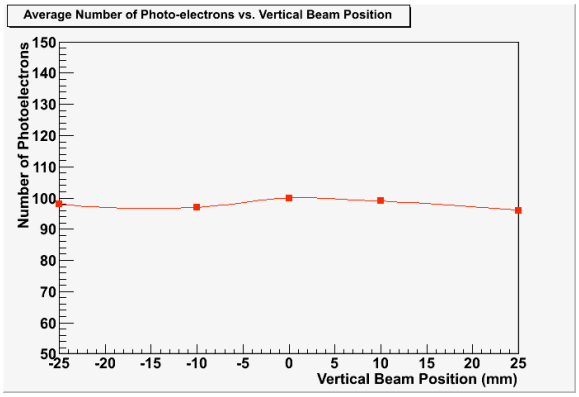

Figure 24: Number of photoelectrons versus vertical beam position.

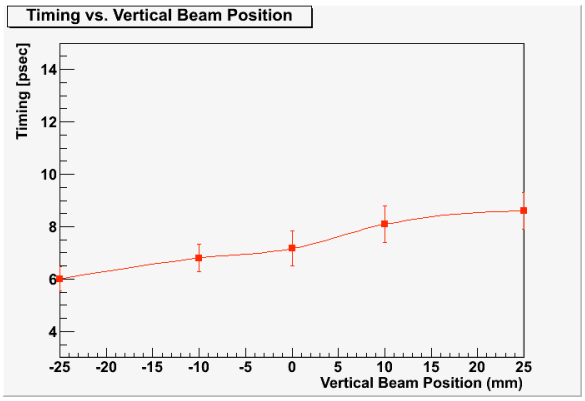

Figure 25: Timing resolution versus vertical beam position

iv. Aerogel Simulations

For the aerogel simulation, the experimental layout used in a test beam experiment done at Fermilab was used as the simulation set-up. The initial set-up used a 4 cm x 4 cm x 1.1 cm aerogel (SiO_2) tile. Adjacent to the tile was a plane mirror with an elliptical cross-section tilted at 45 degrees as shown in figure 26. Adjacent to the mirror and aerogel tile was a circular Photek 240 of diameter 4.1 cm also shown in figure 26. As represented by the horizontal blue line, an incident beam 200GeV protons was directed at the center of the aerogel tile, which radiated cerenkov light at approximately 14 degrees relative to the incident beam line. The cerenkov light leaving the radiator, reflects off the mirror and unto the detector.

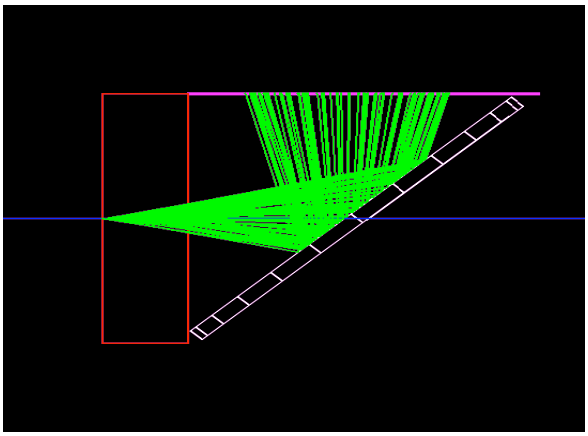

Figure 26: A diagram showing the initial layout of the aerogel simulation. An incident beam of 200 Gev protons, represented by the blue line, was incident on on a single aerogel tile of 4 cm x 4 cm x 1.1 cm dimensions (shown in red). The cerenkov light (green) is generated in the aerogel and is reflected off the a plane mirror shown and directed into a Photek 240 detector (purple) that has a diameter of 4.1 centimeters. The optical path length from the edge of aerogel tile (facing the mirror) to the detector is 4 cm.

Figures 27 and 28 show the optical properties of aerogel. Figure 27 shows the absorption length of aerogel versus wavelength. One should make not of the scale of y axis, which ranges from approximately 61.719 cm to 61.721 cm. Hence, for practical purposes, one can assume that the absorption length of aerogel remains constant over the visible wavelength range. Dispersion is also negligible over the visible spectrum, so we assumed a constant refractive index of 1.0306 [4]. Figure 28 shows the scatter lengths of aerogel as a function of wavelength. Here one can see a significant variation in the scatter lengths where at approximately 200 nm the scatter length is a few millimeters while at the red end of the spectrum the scatter length is around a meter. This would suggest that Rayleigh scattering would be a significant factor for cerenkov photons at the blue/ultraviolet end of the spectrum. Aside from the aforementioned properties, all other physics properties remained the same as before.

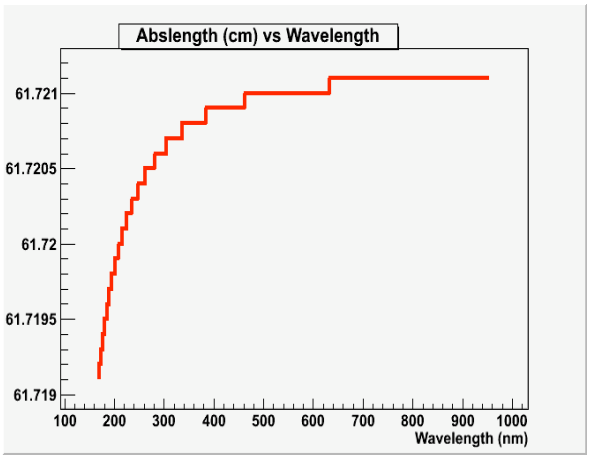

Figure 27: Absorption length (cm) against wavelength (nm) for aerogel

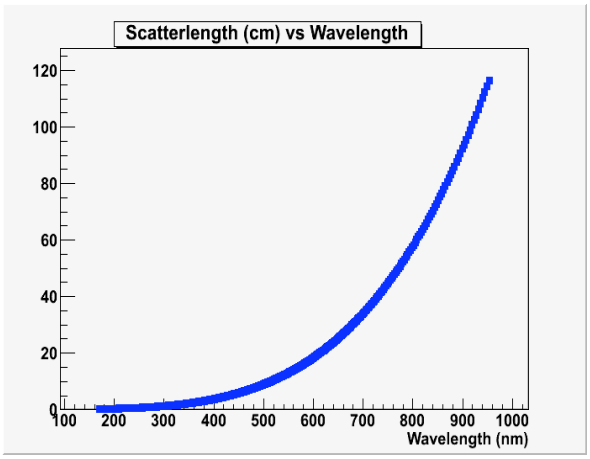

Figure 28: Scatter length (cm) versus Wavelength (nm) for aerogel.

The Photek detector had the same properties as it did in the quartz bar simulations, i.e. with the same quantum efficiency (see fig. 5) , LCE of 60%, gain of 100 and time transit spread of 30 picoseconds. The timing resolution was obtained using the DCOG method, which was previously explained. As with the quartz bar simulations, analyses of the cerenkov photons were taken at different stages of simulation.

The first simulation was done using a single 4 cm x 4 cm x 1.1 cm aerogel tile. The photon spectrum, photon hits, number of photoelectrons, arrival time, and timing resolution at the detector were obtained. Next, a second aerogel tile of the same dimension was stacked in front of the previous tile. The photon spectrum, photon hits, number of photoelectrons, arrival time, and timing resolution at the detector were again obtained. The same was done for a third and fourth aerogel tile. To investigate the effect of Rayleigh scattering, the entire process was repeated with Rayleigh scattering turned 'off' in the simulation. The final aspect of aerogel simulation was to vary the position of the detector. The optical path length of the cerenkov light was varied from 4.0 cm to 4.5 cm. in steps of 1 mm. The average number of photoelectrons, arrival time and timing resolution were taken for each step.

v. *Results of Aerogel simulation*

Figure 29 shows the photon hits at the detector for the initial set up with one 1.1 cm aerogel tile. The scatter plot shows a well defined ring that is contained within the surface area of the photek detector. Figure 30 shows the number of photoelectrons generated at the detector for 1000 events with the average being approximately 6 per event. Figure 31 shows the resulting distribution of arrival times for 1000 events with the timing resolution being approximately 8.1 picoseconds.

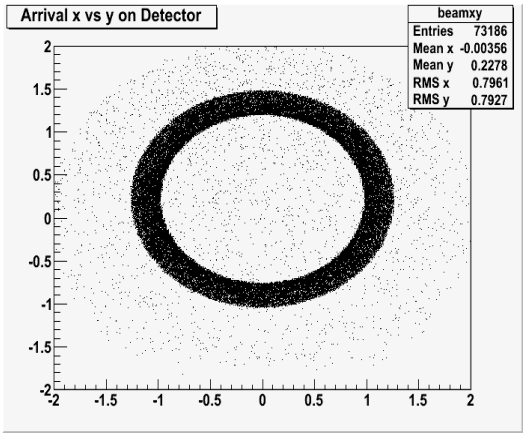

Figure 29: Photon hits at the detector.

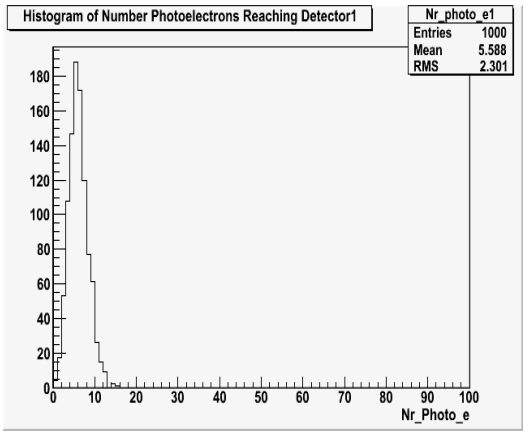

Figure 30: Histogram showing the number of photoelectrons per event for 1000 events.

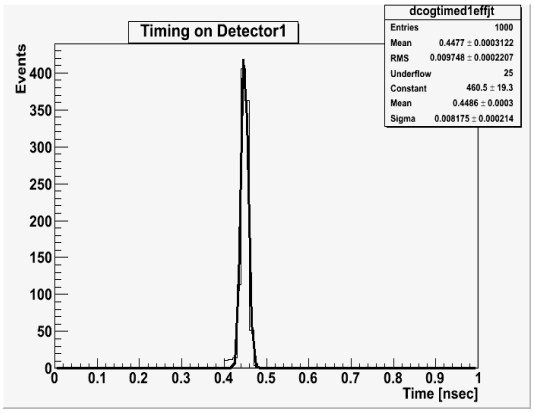

Figure 31: A plot showing the spread of the arrival times for the case one 1.1 cm aerogel tile. The timing resolution obtained in this case approximately 8.1 picoseconds.

Figures 32 through 35 show the photon hits on the detector for two, three, and four aerogel tiles respectively. From these scatter plots one observes

that the thickness of the ring increases with the thickness of the aerogel. Another important thing to note is the decrease in photon density around outer the regions of the rings.

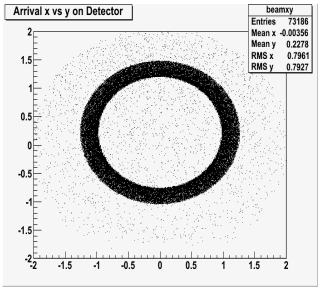

Figure 32: Photon hits for 1 x 1.1 cm aerogel tile.

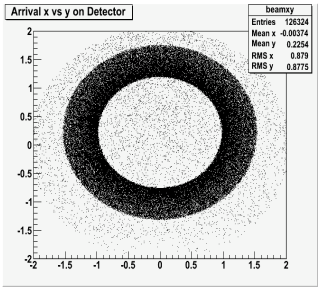

Figure 33: Photon hits for 2 x 1.1 cm aerogel tile.

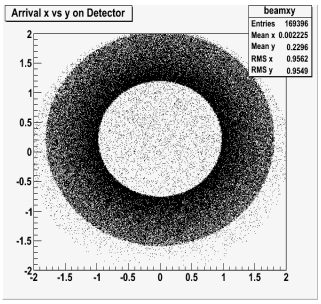

Figure 34: Photon hits for 3 x 1.1 cm aerogel tile.

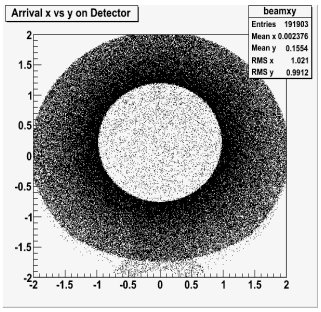

Figure 35: Photon hits for 4 x 1.1 cm aerogel tile.

Figure 36 shows that as the total tile thickness is increases, the number of photoelectrons increases. However, this increase begins to level off at greater tile thickness. A similar effect is observed observed with the timing resolution, which improves as the total tile thickness is increased but begins to level off at higher tile thickness as seen figure 37.

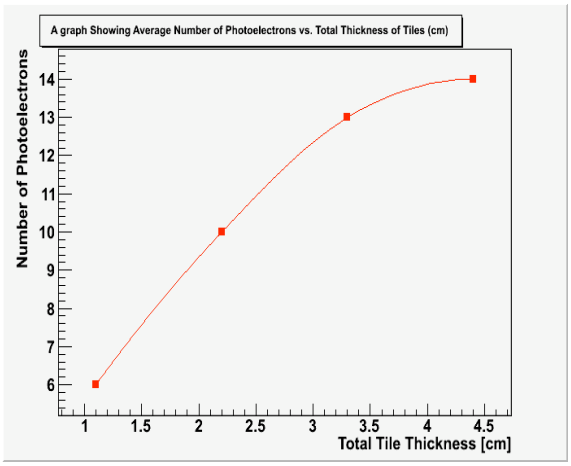

Figure 36: Number of photoelectrons versus total tile thickness for aerogel

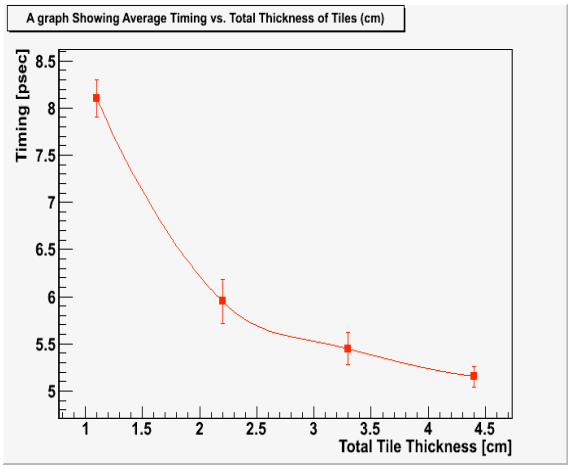

Figure 37: Timing resolution versus total thickness for aerogel

Figure 38 shows a comparison of the wavelength spectra with and without the presence of Rayleigh scattering for the cases of one, two and three aerogel tiles. In all cases, there was a significant difference in the number of photons present in the blue end of the wavelength. This was most dramatic for the case of 3 aerogel tiles. Figure 39 shows another perspective on the effect of wavelength scattering. This plot shows the result of dividing the wavelength spectrum with rayleigh scattering by the wavelength spectrum without rayleigh scattering. For the case of three aerogel tiles, rayleigh scattering accounts for a maximum of about 75% loss of photons in the blue range of the wavelength spectrum.

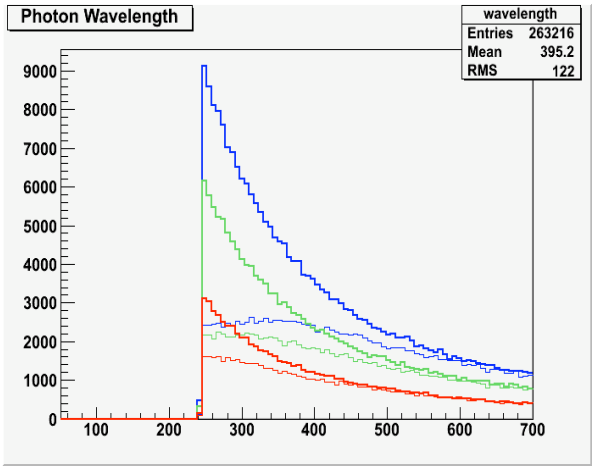

Figure 38: These plots are a comparison of photon wavelength spectra arriving at the detector for the cases of one (red), two (green) and three (blue) 1.1 cm Aerogel tiles. The bold lines represent the simulated wavelength spectrum in the case of no Rayleigh Scattering and the thin lines represent the spectrum with Rayleigh Scattering.

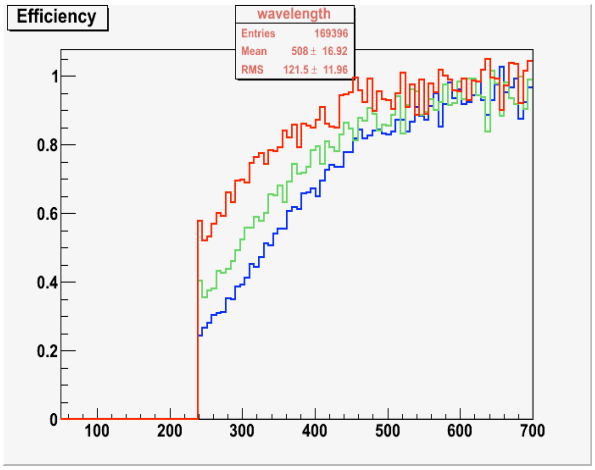

Figure 39: represents the wavelength spectrum of the proportion of photons that reaches the detector after Rayleigh Scattering. The color coding is the same as in figure 38.

Figure 40 and 41 show the result of varying the optical path length of the light between the surface of the aerogel radiator and the Photek detector. Fig. shows the number of photoelectrons against the optical distance, which was constant at around 13 photoelectrons for an optical distance range of 4.0 to 4.5 cm. Subsequently, the timing resolution showed little variation and remained between 5 and 6 picoseconds as shown in figure 41.

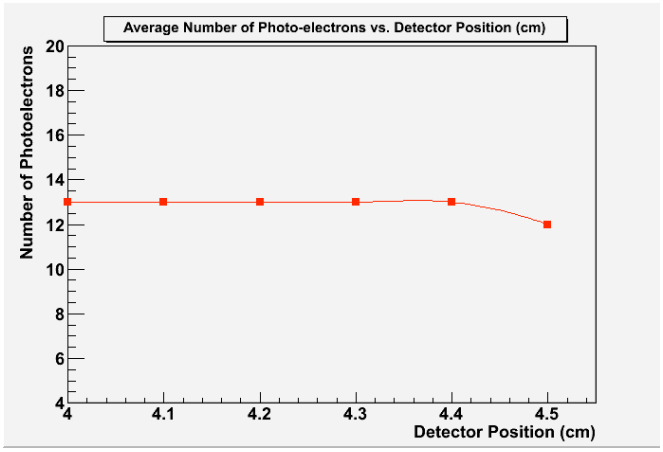

Figure 40: Number of photoelectrons versus optical path length.

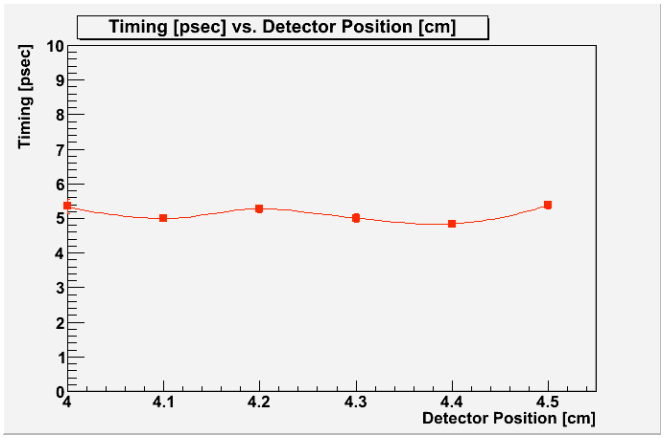

Figure 41: Timing resolution versus optical path length.

IV. DISCUSSION

This section will analyze and discuss the key aspects of quartz bar and aerogel simulation results. From figures 11 and 12, one can observe that secondary photons are usually produced in much fewer numbers than primary photons. Moreover, the simulation shows that it is most likely the case that no secondary photons will be generated for a given event. However, as figure 12 emphasizes, for a given - albeit uncommon - event, it is possible to have more secondary photons than primary photons. In such an event, these significant number of these photons could arrive before the primary photons,

skewing the timing of the detector. This result would underlines the fact that secondary photons remain a significant factor that needs to be taken into account.

One way to minimize or possibly eliminate the interference of secondary photons is to have the quartz bar tilted at the cerenkov angle. At this angle, most of the cerenkov light emitted on one side of the beam will travel in a straight line directly to the detector. This essentially eliminates the possibility of having a large number of the secondary photons arriving before primary photons, thus improving the timing resolution. Figure 15 shows this to be true. As the angle of incidence increases, the timing resolution also increases but continues to do so even beyond the cerenkov angle going to low of about 2.8 picoseconds at 65 degrees. The reason for lies in figure 14 which shows the number of photoelectrons against angle of incidence. As the angle increases, the proton travels through more of the quartz, generating more cerenkov photons, which in turn produces more photoelectrons. At an incident angle of 0 degrees, the photek detector generated approximately 50 photoelectrons but at 60 degrees, the number of photoelectrons increases approximately 3 fold to 150 photoelectrons. Based on the statistically nature of the timing resolution, this will naturally lead to a better timing resolution. Nevertheless, one would not expect to see a timing resolution of 2.8 picoseconds experimentally. After dispersion and light collection efficiency were added, the timing resolution was revised. As expected, the timing resolution got worse. For the case when the proton beam was perpendicular to the quartz bar, the timing resolution increased from 7 picoseconds to 15 picoseconds after dispersion and a 60% light collection efficiency was added.

The simulations also met expectations when the dimensions of the quartz bar were varied. As the length of the quartz bar increased, the number of photoelectrons generated at the detector decreased and as a result the timing resolution got worse. This is expected considering that the cerenkov photons had to travel traveling through more of the material, making them more likely to get absorbed. As the thickness of the tile increased, the number of photoelectrons increased and as a result the timing resolution improved. Again, this should be expected seeing that more cerenkov photons are emitted as proton travels through more of the material.

Varying the position of the incident beam also proved to have a relatively small effect on the timing resolution. As the position of the proton beam was varied across the horizontal plane, the number of photoelectrons at the detector remained approximately constant and so did the timing resolution. With the incident angle set at the cerenkov angle, the path for the photons to get to the detector does not change much, so very little change in the timing resolution is expected. The same logic can apply to the case of varying the position of the beam vertically although there was a slightly greater variation in the timing resolution.

The aerogel simulation yielded very insightful results into the physical process of the aerogel test beam experiment. Of particular interest was the effect of Rayleigh scattering. As figure 36 shows, as subsequent aerogel tiles were added, the number of photoelectrons increased but by fewer amounts with each additional tile. This is due to the fact Rayleigh scattering becomes more significant as the optical path through the aerogel material increases. A closer look at the wavelength spectrum reveals that Rayleigh is most predominant in the blue region of the wavelength spectrum as shown by figure 38. This is to be expected given the scatter length spectrum shown in figure 39. Varying the optical path length of the cerenkov photons had very little effect on the timing resolution. This is not surprising considering the size of the cerenkov ring was still contained within surface area of the detector. However, one would expect a drop in the number photoelectrons at greater optical path lengths as the ring size would get to large to be fully contained within the detector.

V. CONCLUSION

The quartz bar and aerogel simulations yielded very useful results, which brought about a greater understanding of how these materials can be used in a detector set up. With the quartz bar, we learnt that increasing the angle incidence of the incoming proton beam slightly past the cerenkov angle produces better timing resolution. The prevailing factor seemed to be the overall increase in the number of photoelectrons generated. This is corroborated by the simulation result which showed that increasing the overall thickness of the quartz bar yields a better timing resolution. Our simulation also showed that the Photek 240 gets a much timing resolution than the Hamamatsu due to its better sensitivity to light in the blue/ultra-violet region of wavelength spectrum. We also learn that when the incident angle set at the cerenkov angle is very robust against minor changes in the beam position as the very little changes in the timing resolution were observed when the position of the beam was varied +/- 2.5 cm in both the horizontal and vertical positions. With aerogel, we learn that Rayleigh scattering has a very predominant effect on the timing resolution, particular in the blue region of the wavelength spectrum. We also learn that varying the optical path length of the photons has very little effect on the timing resolution as long as the cerenkov ring stays within the detector.

From these results we can determine different ways to improve the timing resolution of both detectors. One consideration is to increase the total thickness of the quartz bar either through thicker quartz bars are multiple quartz bars in sequence. From our simulation, we would expect the better timing resolution through an increase in the number of photoelectrons. The same can be applied to the aerogel set-up but to a much lesser extent due to the predominant effect of Rayleigh scattering.

However, much more can be done to improve the quality of our simulations. Our simulated timing resolution is still significantly better than what has been observed experimentally. While it is evident that a simulation is relatively free from systematic errors that may occur during an actual experiment, much more parameters can be added to the present simulation to create a more realistic environment. Such parameters could be the electronics of the detector. This could involve effects such as electronic jitter, losses along wires and variation in the gain. Such effects are expected to worsen the timing resolution of both set-ups.

Acknowledgments

I would like to acknowledge my advisor, Hans Wenzel, for his dedicated guidance though out the duration of my project. I would like to thank Mike Albrow and Sasha Pranko for all their advice and contributions to this project. Special thanks must go to SIST program committee for giving me the opportunity to do research at Fermilab and to all others who have made this research possible.

References

[1] M.G. Albrow et al. (FP420 R and D Collaboration), arXiv:0806.0302.

[2] Geant4: Nuclear Instruments and Methods in Physics Research, Section A, Vol. 506
(2003) 250-303, and IEEE Transactions on Nuclear Science, Vol. 53, No. 1 (2006) 270-
278.

[3] Rene Brun and Fons Rademakers,
ROOT - An Object Oriented Data Analysis Framework, Proceedings AIHENP'96 Workshop, Lausanne, Sep. 1996, Nucl. Inst. & Meth. in Phys. Res. A 389 (1997) 81-86.

[4] T. Bellunato et al. (Refractive Index Dispersion Law of Silica Aerogel), Eur. Phys. J. C 52, 759-764 (2007).